# Letters

## Small-Signal Equivalent Circuit Model of Quasi-Square-Wave Flyback Converter

Zhemin Zhang, *Student Member, IEEE*, Shuilin Tian, and Khai D. T. Ngo, *Fellow, IEEE*

***Abstract*—One benefit of switching a converter at very high frequencies—even to the multimegahertz range—is that the loop bandwidth can be increased so that the transient performance is significantly improved. However, using the conventional small-signal model of continuous conduction mode (CCM) for quasi-square-wave (QSW) converters introduces a huge mismatch for the placement of the dominant poles when compared to the experiment results. The double poles in high-frequency QSW converters are split widely which cannot be predicted by the conventional model. A modified small-signal model of the QSW flyback converter is proposed to predict the double-pole splitting phenomenon and to analytically quantify the damping effect. The impacts of deadtime on control-to-output transfer function have been investigated in detail. The conventional CCM model turns out to be a special case of the proposed model. The theoretical analyses were eventually verified by Simplis simulation and experimental results on a 5-MHz QSW flyback converter.**

***Index Terms*—Damping effect, deadtime, small-signal equivalent model, quasi-square-wave (QSW) converter.**

### I. Introduction

With the fast development of telecom, computer, and network systems, power consumption and volume reduction are desired. A typical method for achieving high power density involves increasing the switching frequency and operating the converter in quasi-square-wave (QSW) mode or critical-conduction mode (CRM) to minimize switching loss and noise [1]–[5]. Another benefit of switching a converter at very high frequencies, even to the multimegahertz range, is that the loop bandwidth can be increased so that the transient performance is significantly improved.

In the conventional small-signal model of PWM converter, the rising time and falling time of PWM switch are negligible for both continuous-conduction mode and discontinuous-conduction mode [6], [7]. However, for QSW converter at high switching frequencies in particular, the time interval that the inductor resonates with the output capacitance of the switches cannot be neglected. The driver's deadtime or resonant interval has significant influence on the transfer function of the power stage [see Figs. 1(b) and 5]. Therefore, the traditional small-signal model in [6] and [7] cannot predict the transfer function in QSW mode operation. There is no small-signal equivalent circuit of CRM or QSW converter, so that the design of compensator only depends on simulation [2], [8]. The circuit averaging method was adopted in [9] to obtain the small-signal model in critical load condition for a buck converter, but the control-to-output transfer function is not obtained analytically.

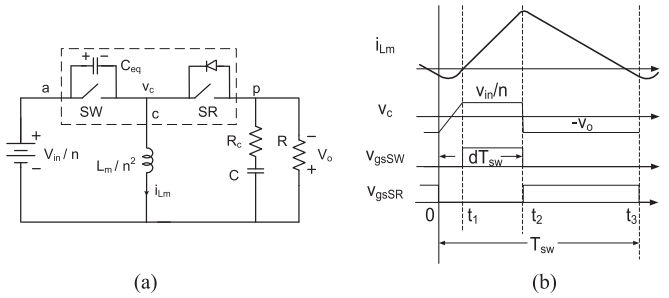


(a) (b)

Fig. 1. (a) Schematic of QSW buck–boost converter and (b) typical waveforms.

A QSW small-signal equivalent circuit model is proposed in this letter. The proposed model is a big improvement upon the conventional model by quantifying the damping effect as a result of the resonant interval. The conventional model is proved to be a particular case (when deadtime is zero) of the proposed model. A 5-MHz QSW flyback converter was fabricated to validate theoretical analysis, and the dynamic performance is improved significantly with an accurate small-signal model.

### II. Derivation of Small-Signal Model for QSW Flyback Converter

A modified small-signal model is derived in this section to address the double-pole splitting phenomenon for QSW flyback converter. The methods used here are also applicable for other QSW converters. To simplify the analysis, the components on the primary side of the flyback converter are transferred to the secondary side with respect to the turns ratio, which is equivalent to buck–boost converter shown in Fig. 1(a). The leakage

Manuscript received October 22, 2016; revised November 19, 2016 and December 27, 2016; accepted January 15, 2017. Date of publication January 30, 2017; date of current version March 24, 2017. This work was supported by Texas Instruments.

The authors are with the Center for Power Electronics Systems, The Bradley Department of Electrical and Computer Engineering, Virginia Tech, Blacksburg, VA 24061 USA (e-mail: zzhang70@vt.edu; tianshuilinpe@gmail.com; kdtn@vt.edu).

Color versions of one or more of the figures in this paper are available online at http://ieeexplore.ieee.org.

Digital Object Identifier 10.1109/TPEL.2017.2661320

inductance is in series with magnetizing inductance. Since the coupling of transformer is easily greater than 97% in practice, the leakage inductance is negligible. The functional block represents the total nonlinearity in these converters, and is shown as a three-terminal nonlinear device. The terminal designations a, p, and c refer to active, passive, and common, respectively. The equivalent capacitance $C_{\rm eq}$ is the sum of the output capacitance of SW and SR.

The typical waveforms of QSW converter are shown in Fig. 1(b). During interval $[0,\ t_1]$, the inductor resonates with equivalent capacitor $C_{\rm eq}$ to discharge the stored energy and achieve ZVS for SW. The turn-OFF current for SW is much higher than the turn-OFF current for the SR, which means the resonant interval needed to charge $C_{\rm eq}$ is much shorter and it can be ignored.

In the conventional PWM switch model, the switch voltage $v_c$ [see Fig. 1(a)] is assumed to follow the control signal exactly without delay. Fig. 1(b) shows that during interval $[0,\ t_1]$ the switch-node voltage waveform $v_c$ does not remain constant under different input or load conditions due to the resonance. Therefore, the influence of this resonant interval on the small-signal analysis needs to be investigated, and the circuit averaging method is adopted here to derive the small-signal model for the QSW converter.

According to the waveform in Fig. 1(b), the instantaneous switch node voltage $v_c$ at each interval can be expressed by

$$v_c\left(t\right)=\begin{cases}-V_o\cos\omega t-Zi_{\rm Lm}\left(0\right)\sin\omega t & 0<t<t_1\\ V_{\rm in}/n & t_1<t<t_2\\ -V_o & t_2<t<t_3\end{cases}\tag{1}$$

where $\omega=\frac{n}{\sqrt{L_m\,C_{\rm eq}}}$ and $Z=\frac{1}{n}\sqrt{\frac{L_m}{C_{\rm eq}}}$. The initial inductor current $i_{\rm Lm}\left(0\right)$ at time zero is close to the valley current, which can be derived as

$$i_{\rm Lm}\left(0\right)=i_{\rm Lm}-\frac{n^2V_o\left(1\ -\ d\right)T_{\rm sw}}{2L_m}\tag{2}$$

where $i_{\rm Lm}$ is the average inductor current. Integrating (1) over the course of one switching cycle yields the average phase node voltage as follows:

$$\begin{aligned}v_c=&\frac{V_{\rm in}\left(dT_{\rm sw}-t_1\right)}{nT_{\rm sw}}-\frac{v_o\left(1\ -\ d\right)}{2}\left(1+\cos\omega t_1\right)\\&-\frac{v_o\sin\omega t_1}{\omega T_{\rm sw}}-\frac{Zi_{\rm Lm}}{\omega T_{\rm sw}}\left(1-\cos\omega t_1\right).\end{aligned}\tag{3}$$

To apply the small-signal perturbation and linearization of $v_c$, $d$, $v_o$, and $i_{\rm Lm}$, the small-signal model can be obtained as

$$\widehat{v_c}=K_d\hat{d}-K_o\widehat{v_o}-R_{\rm res}\widehat{i_{\rm Lm}}\tag{4}$$

where

$$R_{\rm res}=\frac{L_m\left(1-\cos\omega t_1\right)}{n^2T_{\rm sw}}.\tag{5}$$

For most practical applications, $R_{\rm res}$ is large enough to have a significant impact on the control-to-output transfer function. The resonant terms in $K_o$ and $K_d$ are relatively small compared to static terms, and can be simplified as

$$K_o=\frac{1\ -\ D}{2}\left(1+\cos\omega t_1\right)+\frac{\sin\omega t_1}{\omega T_{\rm sw}}\approx1-D\tag{6}$$

$$K_d=\frac{V_{\rm in}}{n}+\frac{V_o}{2}\left(1+\cos\omega t_1\right)\approx\frac{V_{\rm in}}{n}+V_o.\tag{7}$$

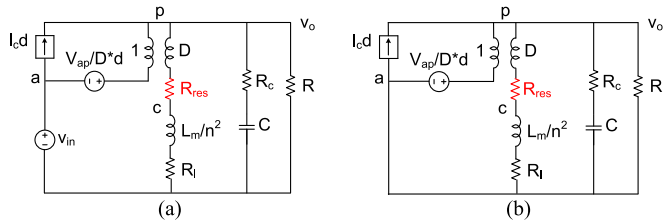


Fig. 2. (a) Small-signal model including damping resistor for QSW converter and (b) SMall-signal equivalent circuit for control-to-output transfer function.

Using PWM switch model, the small-signal equivalent circuit including damping resistor for QSW converter is shown in Fig. 2(a). To derive the control-to-output transfer function, the input voltage source is shorted to ground; the equivalent circuit is derived and shown in Fig. 2(b).

Due to the small magnetizing inductance in the QSW converter, the right half-plane zero moves beyond half of the switching frequency, which has a trivial impact on the transient response, in contrast to the conventional flyback converter. Therefore the circuit-oriented control-to-output transfer function of the QSW converter can be expressed as

$$\frac{v_o}{v_{\rm ctrl}}=\frac{k_m\,G_{\rm do}\left(1+s/s_{z1}\right)}{1+s/\omega_0Q+s^2/{\omega_0}^2}\tag{8}$$

where $k_m$ is the modulation gain; D' = 1-D;

$$G_{\rm do}=\frac{V_{\rm in}}{nD'^2}\tag{9}$$

$$s_{z1}=\frac{1}{R_cC}\tag{10}$$

$$\omega_0\approx\frac{nD'}{\sqrt{L_m\,C}}\tag{11}$$

$$Q\approx\frac{D'}{n\left(D'^2R_c+R_l+R_{\rm res}\right)}\sqrt{\frac{L_m}{C}}.\tag{12}$$

When quality factor Q of the converter is greater than 0.5, the dominant poles in the denominator of (8) are complex-conjugate. On the other hand, the double poles will split and become two real poles when Q is smaller than 0.5. As shown in (12), the value of Q is highly dependent upon the small-signal damping resistor.

## III. Impact of Deadtime on Control-to-Output Transfer Function

The impact of deadtime has on the power stage control-to-output transfer function is discussed in this section. Given the specifications of nominal input voltage $V_{\rm in}\ =\ 48\,{\rm V}$, full load $P_o\ =\ 30\,{\rm W}$, the key parameters including inductance $L_m$, turns ratio n, output capacitor C, ESR of output capacitor $R_c$, and

TABLE I
VALUES OF PARAMETERS IN QSW FLYBACK CONVERTER

| Parameters | Value |
|---|---|
| Magnetizing inductance $L_m$ | 0.85 $\mu$H |
| Turns ratio n | 4 |
| Output capacitor C | 20 $\mu$F |
| ESR of output capacitor $R_c$ | 2.5 m$\Omega$ |
| Winding resistor $R_l$ | 50 m$\Omega$ |

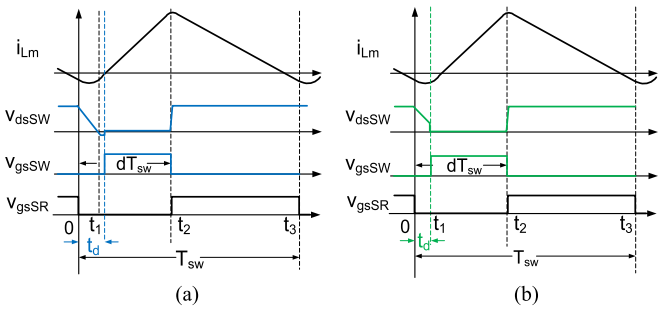


Fig. 3. Waveforms of gate driving with (a) late turn-ON signal and (b) early turn-ON signal.

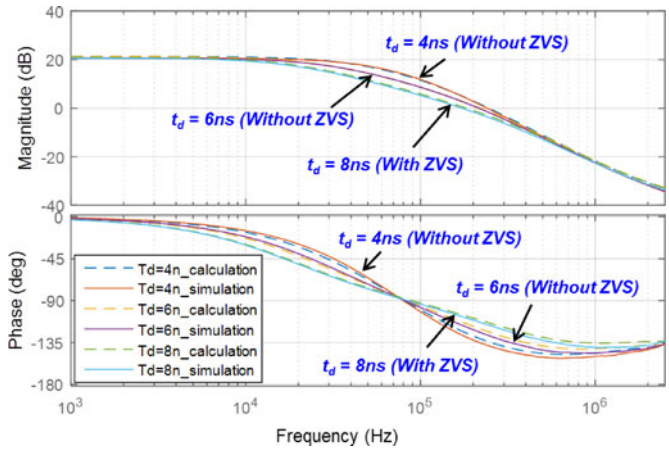


Fig. 4. Control-to-output transfer function of the QSW converter with different deadtimes with $V_{\rm in} = 48$ V, $V_o = 12$ V, $i_o = 2.5$ A, and $f = 5$ MHz.

winding resistors $R_l$ are listed in Table I. The timing of the converter is derived from switch-model based simulation in Simplis.

A short duration of deadtime is required to avoid the shoot-through issue with high current spikes. Due to the limits of the specific device, the temperature, and lot-to-lot variation of the time delay, the deadtime may not be controlled exactly, as shown in Fig. 1(b). The gate-drive signal may be earlier or later than expected, as indicated in Fig. 3. Large turn-ON loss will be induced with early gate driving signal; on the other hand, the voltage drop of body diode for synchronous rectifier may cause extra conduction losses with late drive arrival.

To investigate the impact of deadtime on the control-to-output transfer function of the QSW converter, the Bode plots of different deadtimes with $V_{\rm in} = 48$ V, $V_o = 12$ V, $i_o = 2.5$ A, and $f = 5$ MHz are plotted and shown in Fig. 4. Based on the transient simulation at steady state, the resonant time $t_1$ is 8 ns to

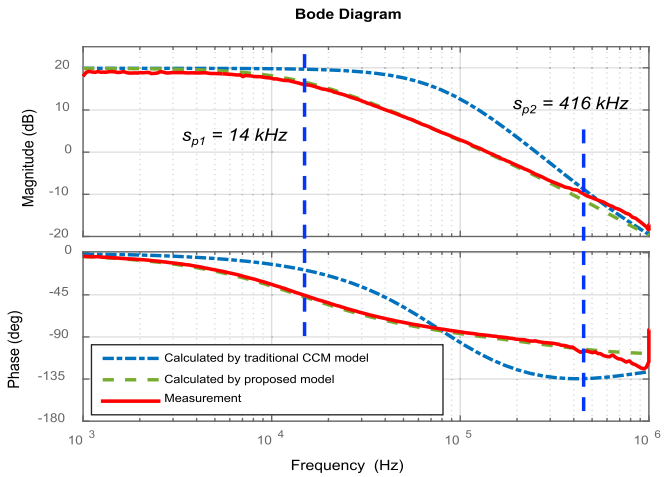


Fig. 5. Calculation and measurement results of control-to-output transfer function for a QSW flyback converter with $V_{\rm in} = 48$ V, $V_o = 12$ V, and $R = 5\,\Omega$.

achieve fully ZVS of input switch. When deadtime $t_d$ is exactly equal to resonant time, the damping resistor can be calculated from (5) as 83.3 m$\Omega$ and the dominant poles are 18and 383 kHz. If the gate signal arrives late as shown in Fig. 3(a), the body diode is conducting, and the control-to-output transfer function will not change. But if the driving signal is earlier as 6 ns, the damping resistor will increase to 48 m$\Omega$ and the poles are split to 25 and 270 kHz; When $t_d$ is 4 ns, $R_{\rm res}$ is derived as 21.7 m$\Omega$ and the real poles are located at 38 and 179 kHz. As deadtime changes from 4 to 8 ns, resistance increases 3.8 times, and the damping is much stronger.

When $t_d$ is equal to zero, $R_{\rm res}$ will be zero as well, according to (5), and the model will be equivalent to the conventional continuous conduction mode (CCM) model. After running the ac analysis in Simplis with the parameters listed in Table I, the control to output voltage transfer function is derived, which shows great agreement to the calculations by using the proposed model for different cases.

## IV. EXPERIMENTAL VERIFICATION

In order to validate the theoretical analysis of the small-signal model of the QSW flyback converter, the open-loop transfer function from control to output was measured with $V_{\rm in} = 48$ V, $V_o = 12$ V, and $R = 5\,\Omega$ using an Agilent—HP 4396B network analyzer. Fig. 5 shows the control-to-output transfer function of the measurements, the calculation results from traditional CCM model and proposed model. With the given specifications and the same parameters shown in Table I, for conventional CCM model without small-signal damping resistor, the complex conjugate double poles are derived as 75 kHz. Using the proposed QSW model, the dominant poles are calculated to be at 14 and 416 kHz, which shows the great agreement to the experimental results.

With the multimegahertz switching frequency of the QSW flyback converter, hypothetically the loop bandwidth can be pushed to be much higher than in the conventional flyback converter. The accurate small-signal model of the QSW flyback

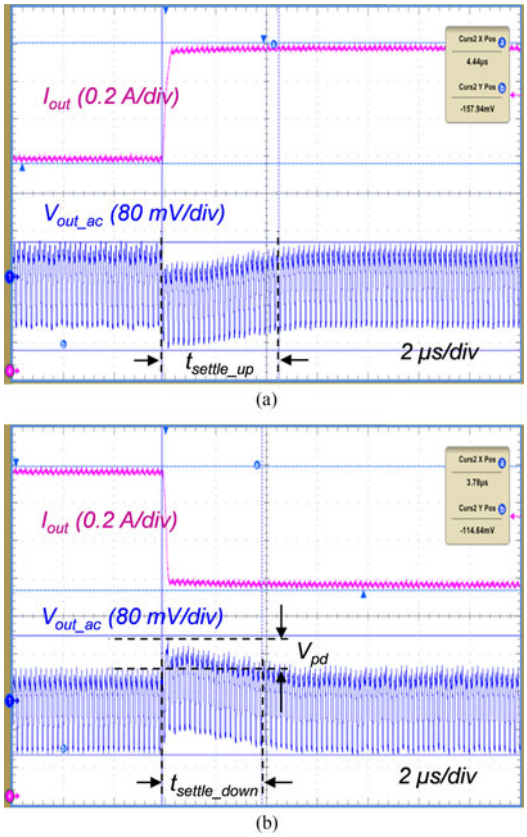


Fig. 6. Experimental load-step response for QSW flyback converter with crossover frequency of 260 kHz, (a) load step-up response and (b) load step-down response.

converter introduced in the previous section helps to realize this higher bandwidth by adding a compensation network afterwards to stabilize the system.

The compensation network is designed to operate with a nominal input voltage of 48 V and under full-load conditions. To boost the phase and push the bandwidth, a Type III compensator is employed. The closed-loop dc gain is boosted by an integrator to minimize the steady-state error. The two low-frequency zeros are to compensate the two dominant real poles, which are placed at 20 and 260 kHz. Two high-frequency poles at 1.9 MHz and 2.23 MHz are used to cancel out the ESR zero and attenuate the switching ripples, respectively. The bandwidth is designed at 260 kHz with an 81° phase margin and 21.6 dB gain margin.

To verify the theoretical analysis of the small-signal model for the QSW converter, a test board was constructed, and a resistive load was built to emulate the load step between 50% and 75% of the full load. The output voltage ripple is relatively large, which is caused by a large current ripple in the QSW converter. To keep the ripple around 100 mV, as it is in the 30-W state-of-the-art commercial flyback converter, the output capacitance is chosen as 20 $\mu$F with an ESR of 2.5 m$\Omega$. The experimental waveforms of $i_{\rm out}$ and $V_{\rm out}$ are shown in Fig. 6 with the crossover frequency at 260 kHz. The dynamic characteristic is quantified by peak derivation and settling times. The parasitic inductance in the PCB or ESL of the capacitor may introduce extra overshoot on the output voltage.

TABLE II
COMPARISON OF TRANSIENT PERFORMANCE OF PROPOSED WORK TO STATE-OF-THE-ART FLYBACK CONVERTER

| | State-of-the-art | Proposed work |
|---|---|---|
| Switching frequency (kHz) | 300 | 5000 |
| Output capacitance ($\mu$F) | 188 | 20 |
| $V_{\rm ripple}$ (mV) | 100 | 94 |
| Designed BW (kHz) | N/A | 260 |
| Step-up settling time ($\mu$s) | 160 | 4.4 |
| Step-down settling time ($\mu$s) | 160 | 3.8 |
| Peak deviation (mV) | 250 | 10 |

By pushing the switching frequency to be approximately 16 times higher, the peak deviation is 15 mV, which is 25 times smaller than in state-of-the-art commercial products. The settling time defined in Fig. 6(a) and (b) is also reduced significantly from 160 to 4.4 $\mu$s for the step-up response, and from 160 to 3.8 $\mu$s for the step-down response. A comparison of the transient performance to that of the commercial flyback converter is summarized in Table II.

## V. CONCLUSION

A modified circuit-oriented small-signal model of QSW flyback converter is proposed in this letter. The model is successfully demonstrated to analyze the damping effect of the resonant time on system double poles. When the resonant time goes longer, the double poles split further. It is verified by simulation in Simplis and experiments of 5-MHz QSW flyback converter. With the help of the proposed small-signal model, the transient performance is improved significantly with high loop bandwidth.

## REFERENCES

[1] X. Huang, F. C. Lee, Q. Li, and W. Du, "High-frequency high-efficiency GaN-based interleaved crm bidirectional buck/boost converter with inverse coupled inductor," *IEEE Trans. Power Electron.*, vol. 31, no. 6, pp. 4343–4352, Jun. 2016.

[2] J. W. Kim, H. S. Youn, and G. W. Moon, "A digitally controlled critical mode boost power factor corrector with optimized additional on time and reduced circulating losses," *IEEE Trans. Power Electron.*, vol. 30, no. 6, pp. 3447–3456, Jun. 2015.

[3] D. Maksimovic, "Design of the zero-voltage-switching quasi-square-wave resonant switch," in *Proc. IEEE Power Electron. Spec. Conf.*, 1993, pp. 323–329.

[4] V. Vorperian, "Quasi-square-wave converters: Topologies and analysis," *IEEE Trans. Power Electron.*, vol. 3, no. 2, pp. 183–191, Mar. 1998.

[5] Z. Zhang, K. D. T. Ngo, and J. L. Nilles, "A 30-W flyback converter operating at 5 MHz," in *Proc. 2014 IEEE Appl. Power Electron. Conf. Exp.*, Fort Worth, TX, USA, 2014, pp. 1415–1421.

[6] V. Vorperian, "Simplified analysis of PWM converters using model of PWM switch. Continuous conduction mode," *IEEE Trans. Aerosp. Electron. Syst.*, vol. 26, no. 3, pp. 490–496, May 1990.

[7] J. Sun, D. M. Mitchell, M. F. Greuel, P. T. Krein, and R. M. Bass, "Averaged modeling of PWM converters operating in discontinuous conduction mode," *IEEE Trans. Power Electron.*, vol. 16, no. 4, pp. 482–492, Jul. 2001.

[8] J. Xue and H. Lee, "Enabling high-frequency high-efficiency non-isolated boost converters with quasi-square-wave zero-voltage switching and on-chip dynamic dead-time-controlled synchronous gate drive," *IEEE Trans. Power Electron.*, vol. 30, no. 12, pp. 6817–6828, Dec. 2015.

[9] W. Qiu, S. Mercer, Z. Liang, and G. Miller, "Driver deadtime control and its impact on system stability of synchronous buck voltage regulator," *IEEE Trans. Power Electron.*, vol. 23, no. 1, pp. 163–171, Jan. 2008.